Conformational, Reactivity Analysis, Wavefunction-Based Properties, Molecular Docking and Simulations of a Benzamide Derivative with Potential Antitumor Activity-DFT and MD Simulations

Jamelah S. Al-Otaibi, Y. Sheena Mary, Y. Shyma Mary, M. Thirunavukkarasu, Ravi Trivedi & Brahmananda Chakraborty

View supplementary material ☐

Published online: 16 Feb 2022.

Submit your article to this journal ☐

View related articles ☐

View Crossmark data ☐

Taylor & Francis
Taylor & Francis Group

Check for updates

Conformational, Reactivity Analysis, Wavefunction-Based Properties, Molecular Docking and Simulations of a Benzamide Derivative with Potential Antitumor Activity-DFT and MD Simulations

Jamelah S. Al-Otaibi[a], Y. Sheena Mary[b], Y. Shyma Mary[b], M. Thirunavukkarasu[c,d], Ravi Trivedi[e], and Brahmananda Chakraborty[f,g]

[a]Department of Chemistry, College of Science, Princess Nourah bint Abdulrahman University, Riyadh, Saudi Arabia; [b]Thushara, Kollam, Kerala, India; [c]Department of Physics, Indo-American College, Cheyyar, Tamil Nadu, India; [d]Department of Physics, Thiru A. Govindasamy Govt. Arts College, Tindivanam, Tamil Nadu, India; [e]Department of Physics, Indian Institute of Technology, Mumbai, India; [f]High Pressure and Synchrotron Radiation Physics Division, Bhabha Atomic Research Centre, Mumbai, India; [g]Homi Bhabha National Institute, Mumbai, India

ABSTRACT

This report aims to study the chemical properties of a benzamide derivative, N-methyl-2-[[3-[©-2-pyridin-2-ylethenyl]-1H-indazol-6-yl]sulfanyl]benzamide (MPSB), having antitumor activities with the help of electronic structure methods. The conformational analysis predicted the lowest energy conformer for the dihedral angle of C16–C14–S1–C11 (45.0^0) of MPSB. UV absorptions in different solvents and air give nearly the same values. The highest delocalization regions are around N5–C21 $=$ O$_2$, C14–S1–C11 and C7 $=$ C8–N3. The reactivity descriptors were discussed in detail to find biological effects. Wavefunction-dependent properties like LOL, ELF, etc. studies provide a lot of information regarding the electronic properties that are ample for predicting bioactivity. Due to the antitumor activity of MPSB, docking is done with different PDBs and 3AGC gives maximum binding energy and the MD simulations of MPSB with 3AGC are analyzed in detail.

Introduction

Due to their broad range of pharmaceutical uses, indazoles have gained considerable interest in the past decades.[1] Indazole moiety is a component of numerous bio-molecules, generating a lot of interest in the new discovery.[2] Many indazole compounds have been well-known for their biological properties for a long time.[3] Indazole scaffolds exhibit fascinating biological characteristics and have gained popularity as a major component in dyes and fluorescent materials.[4–6] All biological molecules have amide functional groups as one of their common properties.[7,8] According to a review of literature, molecules with amide linkages, such as benzamides, need special attention since they exhibit biological and pharmacological properties.[9–11] An indazole derivative synthesis with structure studies is reported by Lu et al.[12] Several benzamide derivatives are effective activators and demonstrated excellent docking poses.[13–17]

Recently, synthesis, biological evaluation, docking and theoretical analysis of novel benzamide derivatives are reported.[18–21] Benzamide derivatives have been successfully designed by several

pharmaceutical companies.[22–24] Molecular modeling of new benzamides with biological activity studies has recently been reported.[25,26] Some medicines, such as celecoxib, apixaban, ibrutinib, crizotinib, axitinib and niraparib having various medicinal effects contain indazole rings.[27–32] Axitinib is an orally active drug used to treat renal cell carcinoma.[33] Axitinib is widely used in conjunction with pembrolizumab or avelumab to treat patients with RCC.[34] Vasileiadis et al.[35] predicted the crystal structures of axitinib. Sulfanyl has the ability to add to a multiple bond intra molecularly and this method has been effectively used in the production of other bioactive chemicals.[36]

The efficacy of a novel benzamide derivative as a chemotherapeutic drug in cancer cells is reported by Narayanan et al.[37] Theoretical methods are reported to understand analytical separations at the molecular level for a benzamide derivative.[38] Zhang et al.[39] reported the design, synthesis and biological evaluation of benzamide derivatives as potential antitumor agents. Routholla et al.[40] reported a series of benzamide derivatives with promising anticancer activity recently. Spectroscopic investigation of some sulfanyl derivatives are reported by the author's group.[41–43]

Metal-organic frameworks have piqued researchers' interest due to their applications in different fields.[44] The structural determination of the gold nanoclusters led to progress in understanding the structure of the gold–ligand interface, the interactions and the methods that control their electrical structure and optical responses.[45] The study of the silver cluster's NLO properties in various solvents shows that they could be used in chemical and pharmaceutical fields.[46] Coinage metal nanoclusters have attracted interest in recent years due to the availability of atomic level precision via combined experimental and theoretical methods.[47,48] In the present study, the DFT, docking and MD simulations of axitinib (MPSB) are reported due to its important biological activities. We report the chemical reactivity descriptors and evaluation of the intra-molecular electron delocalization due to hyper conjugation and other quantum mechanical parameters also.

Methods

DFT calculations have been used for the optimization of MPSB using Gaussian 16,[49] with B3LYP/6-311++G(d,p) basis set (Figure 1).[50] GaussView, Version 6.1 is used for the preparation and viewing of input/output files.[51] The default settings were used for the convergence criteria regarding SCF and optimization procedure. The same basis set is used for conformational analysis, FMOs, MEP and TD-DFT calculations. Reaction sites of MPSB were calculated using Multiwavefunction software.[52] The topological characteristics of ELF, LOL and atoms in molecules (AIM) studies were done using the Multiwfn 3.6 program, which is a key component of Bader's AIM hypothesis. The complex was subjected to MD simulation by Gromacs-2019.4.[53] The system preparation was according to literature.[54] Trajectory analysis for 100 ns was performed to
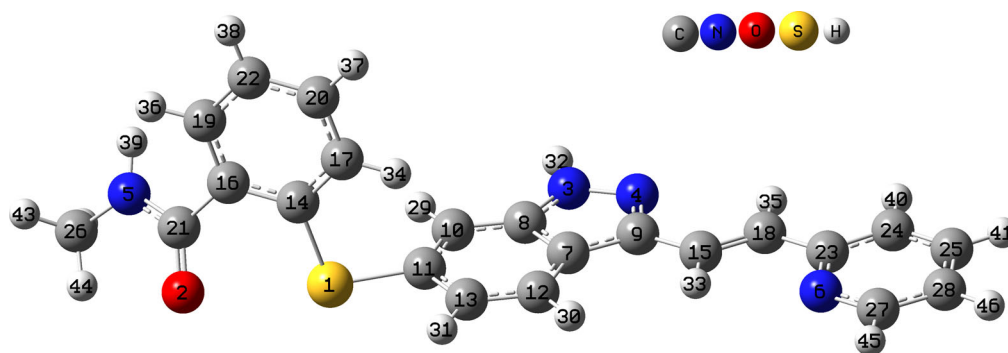

Figure 1. Optimized geometry of MPSB.

find various parameters.[55] MM-PBSA approach was used to find binding free energy with the help of GROMACS utility g_mmpbsa for the last 20 ns in with dt 1000 frames.

The interaction of metal-metal dimer with biomolecule is carried out by Vienna Ab initio Simulation Package 'VASP'.[56,57] We used ab initio projector augmented wave method[58] and a plane wave basis set within the spin-polarized DFT and the generalized gradient approximation[59] for the exchange-correlation energy as implemented in VASP code. To reduce the interaction between the system and its periodic images, all simulation cells were padded with a vacuum space such that there was at least 10 Å of vacuum in all directions between the surface atoms in a cluster and its periodic images. The calculated geometric parameters represent a good approximation and can provide a starting point to calculate other parameters, such as charge distribution using Bader charge analysis, and density of states. The minimum energy structures of interaction of MPSB with Ag–Ag and Au–Au is presented in Figure S1. The validation of optimized structure as a local minimum on potential energy surface (PES) is done by frequency calculations. There is no imaginary frequency.

Results and discussion

Conformational analysis

Conformations are the various spatial arrangements that a molecule can adopt as a result of rotation about a particular bond.[60] The rotation requires activation energy, which is plotted in the PES. The PES is a graphical representation of the energy of a molecule and its geometry.[61] The molecule's most stable conformer was determined using conformational analysis. The PES was generated by finding the total energy with change in dihedral angles, C12–C7–C9–C15, C16–C14–S1–C11, C9–C15–C18–C23 and C16–C21–N5–C26, selected at intervals of 10° by the DFT method (Table 1, Figures S2 and S3). For the conformations, $\tau(1)$ and $\tau(3)$, only one global minimum is observed at 0.0° with energies, −1525.548340 Hartree. $\tau(4)$ produces two minima at 0.0 and 157.0° in which the lowest conformation corresponds to 0.0. $\tau(2)$ produces three minima at 45.0°, 0.0° and 141.0° in which the lowest conformation corresponds to 45.0°. According to PES, conformer $\tau(2)$ was the most stable of all with the lowest potential energy at an angle of 45.0°.

Chemical and electronic properties

The frequency calculations revealed that no imaginary vibrational frequency existed for MPSB, indicating a true minimum. The electronic and geometrical properties of MPSB were investigated using dipole moment values. The FMOs (Figure 2) are undergone chemical reactions due to electron transfers from occupied to the unoccupied molecular orbitals. HOMO is delocalized over phenyl rings while LUMO is over pyridine and indazole rings which are evident for the charge transfer within the system. The different chemical descriptors are (eV): EHOMO = −7.4648, ELUMO = −5.5290, energy gap = 1.8358, hardness = 0.9679, chemical potential = −6.4969 and electrophilicity index = 21.80 eV.[62] The value of electronegativity and hardness are a measure of the capacity of the molecule to attract electrons and the resistance of an atom to charge transfer.

Table 1. Relative energy for different conformations.

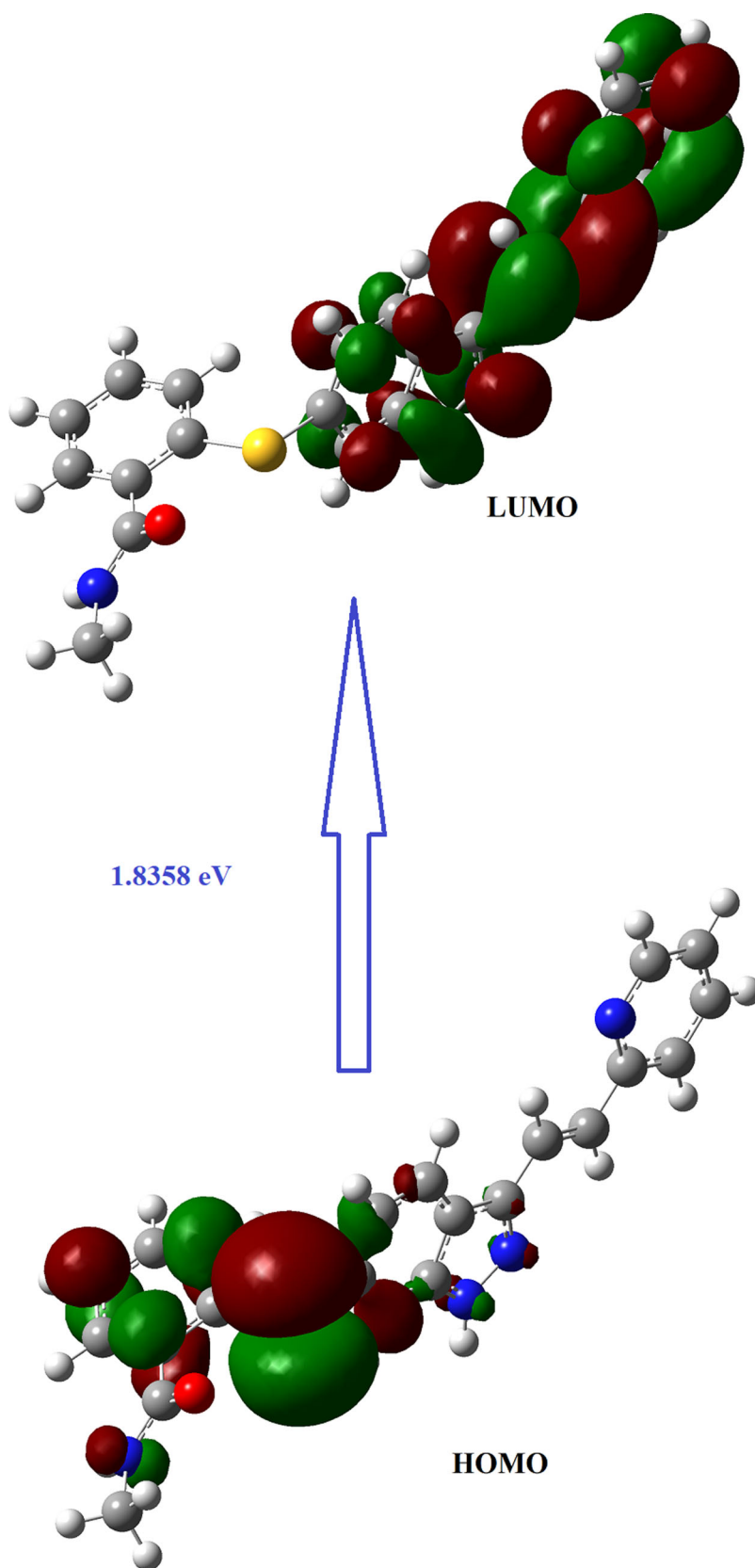|	Dihedral angle	Value (°)	Energy (Hartree)	Relative energy
$\tau(1)$	C12–C7–C9–C15	0.0	−1525.548340	0.000558
$\tau(2)$	C16–C14–S1–C11	45.0	−1525.548898	0.000000
$\tau(3)$	C9–C15–C18–C23	0.0	−1525.548340	0.000558
$\tau(4)$	C16–C21–N5–C26	−0.0	−1525.548340	0.000558

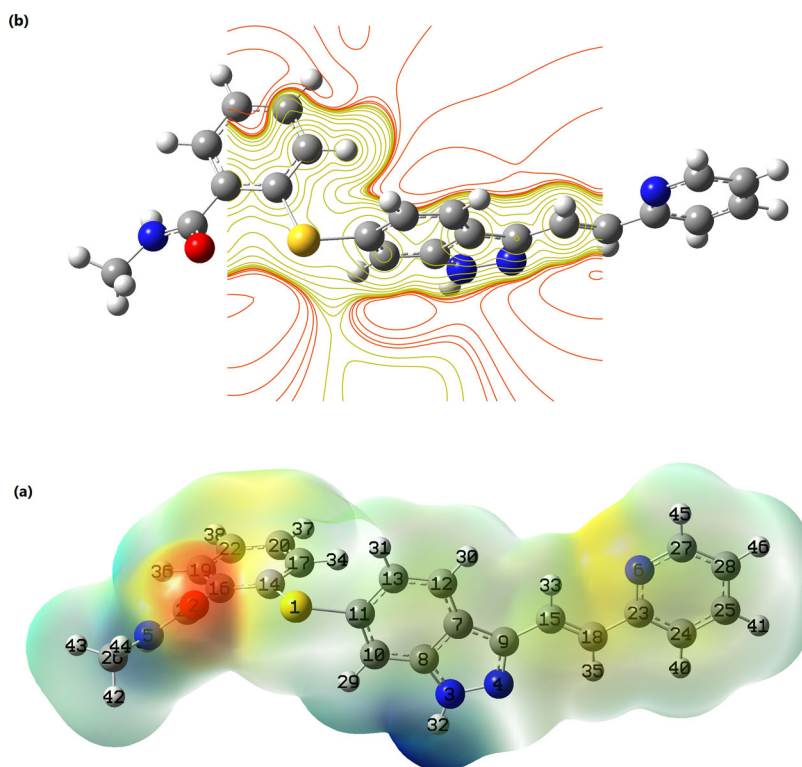**Figure 2.** HOMO-LUMO plots of MPSB.

Figure 3. (a) MEP and (b) ESP plots of MPSB.

The electrophilicity index predicts the stabilization energy when its electrons are saturated and can even be used to predict biological activity.

MEP is employed in biological recognition processes to predict target binding locations, electron donor and acceptor areas.[63] Different colors on the MEP surface (Figure 3) were used to depict the sensitivity of electrostatic potential; intense red and dark blue colors represent high electronegative and electropositive potential. The polarity of the molecule increased as the contrast between red and blue color increased. Non-polarity was shown by the lightening of colors or white shade. Oxygen atoms and the pyridine ring of MPSB were primarily responsible for the red and yellow areas. Higher electronegative and electropositive regions were over O and N, H atoms, indicating sites for nucleophilic and electrophilic attacks.[64]

NBO study is of much interest as it explains the electron shift from bonding to anti-bonding orbitals and in some cases, from anti-bonding to anti-bonding orbitals during chemical reactions. Very strong hyper conjugative interactions are produced by lone pair atoms as[65]: O2→N5–C21, O2→C16–C21, N3→N4–C9, N3→C7–C8, N5→O2–C21 with energies, 22.84, 16.57, 28.85, 37.30, 57.42 kcal/mol. Other interactions are given in Table S1. The high delocalization energies indicate that the molecule is inherently stable due to hyper conjugative delocalization.

In the case of MPSB, the UV absorptions in different solvents and air (Figure S4) are nearly the same (313, 270, 262 nm). Studies using polarizability data is a useful tool to explain the NLO properties of molecules. This helps to identify the suitability of the compound in NLO materials for communication devices. The dipole moment, polarizability, first- and second-order hyperpolarizabilities are 5.302 Debye, 4.654×10^{-23}, $22.033 10^{-30}$ and -42.652×10^{-37} esu, respectively. It can be concluded that the drug molecule can also act as an NLO material.[66]

Charge transfer mechanism

The charge movement component assumes a significant part in bonding communication. In light of the Bader charge examination,[67] we get knowledge into the quantitative assessment of charge move between MPSB and Ag–Ag or Au–Au dimer. As we probably are aware the Ag molecule have $4d^{10}5s^1$ electronic arrangement while Au particle have $5d^{10}6s^1$ electronic design individually and there are all out 11 valence electrons in both case. Here in the current computations, it tends to be seen by Table 1, if Au–Au dimer collaborates with biomolecule, a smidgen around 0.22e charge is moving from the biomolecule to the Au dimer for example Au molecule is in control acquiring state and acting like charge acceptor species while MPSB acts like charge giver species.

Be that as it may, when the Ag–Ag dimer is communicating with biomolecule, there is no charge move between Ag dimer and MPSB. As a rule, our outcomes demonstrate that MPSB will in general, lose electrons on the opposite side, the Ag–Ag dimer incites a higher centralization of electrons at the surface because of the Coulomb interaction region. Another region for inducing charge is spin density, which is preferentially localized around the biomolecule system, not the Ag–Ag and Au–Au dimer.

Density of states

The density of states analysis has also been carried out by using VASP[56,57] for the studied structure. The TDOS plot, a population study per orbital predicts the composition of the molecular orbital in a specific energy range as shown in Figure S5. In the inset, TDOS of MPSB was also calculated by using GauSumm.[68] As we can see, the TDOS plot of pure MPSB shows a larger band gap around 3.80 eV which become 1.12 eV after interacting with Ag–Ag dimer and 2 eV with Au–Au dimer i.e. both the metal dimer making the biomolecule more interactive. A large gap means the system is stable and not suitable for nucleophilic and electrophilic reactions. In the above charge transfer mechanism, we found that Ag–Ag dimmers are gaining charge from the biomolecule that means that the site has more negative charge and will act as the nucleophilic site. The band between −1 to −5eV was formed by the hybridization of C 2p, N 2p, S 3p, O 2p, H 1s and Ag 6s orbitals and also the symmetry between spin up and spin down channel is lost near the Fermi level giving the magnetic signature. The DOS spectra of the Ag–Ag/Au–Au + biomolecule composite near the Fermi level have unequivocal modification as a result of the association of the Ag–Ag/Au–Au dimer. The DOS near the Fermi level is affected through the communication of Ag–Ag/Au–Au on the outer layer of biomolecule and moves somewhere around about 0.76 eV contrasted and the unadulterated MPSB. It makes additional pinnacles show up in the valence band which takes part in the limiting technique. This huge shift can be credited to the lessening in great Coulomb potential on account of the charge move. On the other hand in the case of Au–Au dimmer interaction with biomolecule spin up and spin down channel got adjusted and there is no magnetic signature.

Topology analyses

The atom in molecules theory is a powerful tool for investigating chemical processes on a broad scale and it relies solely on information contained in the electron density and this theory generally provides a way for identifying bonds between atoms in compounds. According to AIM, each pair of atoms that are connected has one bond critical point (BCP) and chemical bonding interactions can be identified and categorized based on the features of the electrons on the critical points and energy densities at these BCPS, also its state that the nature of interaction across the complete reaction route. In general, there are four types of critical points: (3, −3) local maxima or peaks, in which second derivatives must be negative; (3, −1) saddle points or passes (BCPs), at
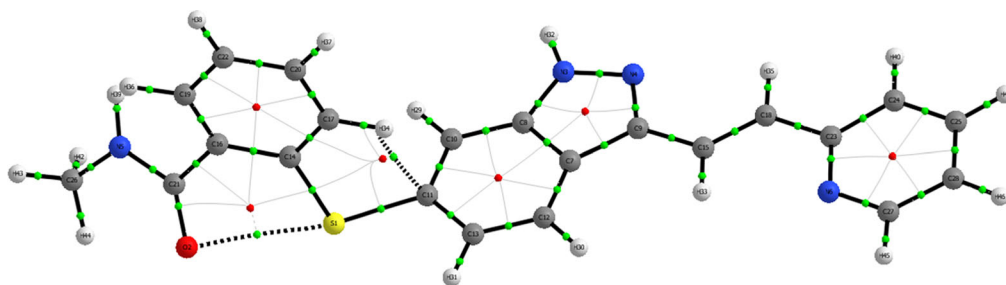
Figure 4. Graphical representation of (a) localized orbit locator (LOL) and (b) Electron localization function (ELF).

which two eigenvectors are negative and the other is one positive; (3, +1) ring critical points or pales, if one is negative and other two are positive; and (3, +3) local minima or pits, in which one is negative and two are positive (cage critical points).[69,70]

In this analysis, only the molecule BCPs were taken into account, the electron density $\rho(r)$ and the second derivative of $\nabla^2\rho(r)$ Laplacian electron density was used to quantify the atomic strength properties and molecular interactions at BCPs respectively. The value of $\rho(r) \geq 0.14$ a.u. and $\nabla^2\rho(r) < 0$, indicates that the shared interactions of covalent bond while the $\rho b(r) \leq 0.05$ a.u., and $\nabla^2\rho(r) > 0$ shows the presence of the closed-shell interactions of ionic, Van der Waals, hydrogen bond etc., at BCPs.[71] Figure 4 shows the AIM molecular graph of MPSB, with bond paths as black lines, critical points as green small spheres), ring path (ash color solid lines), ring critical points RCP's as small red sphere and non-covalent weak interactions (black dotted lines).

The BCP, where the localized attractor of the electron density distributions, was used to determine the topological parameters, and the values are provided in Table S2. From this table the positive value of $\nabla^2\rho(r)$ are 0.0560 and 0.0469 a.u. at S1–O2 and C11–H34 shows that the closed shell weak interactions of electrostatic nature and other negative values of $\nabla^2\rho(r)$ and the range 0.0146 to 0.3259 a.u. of $\rho(r)$ represents a strong covalent bond interaction. The bond ellipticity $\mathcal{E}$, is anisotropy of electron density curvature and measures the π-bond nature, was examined. The strong the π-delocalization and asymmetry of electron density distributions were identified by the greatest value of $\mathcal{E}$.[72,73] In the present case, the highest $\mathcal{E}$ value was noted at C11-H34, which exhibits the greater asymmetry of electron density distribution and π-bond nature of the title compound.

The LOL and ELF were frequently employed to show the relationship between the electronic and geometry structure of the compound. Schmider and Becke's early reported, LOL functions are widely utilized to explain chemical properties such as chemical shell structure, molecular bonding and lone pair electrons and also based on the kinetic energy density, LOL and ELF have a similar interpretation of chemical properties.[74,75] Figures 5 and 6, show a quantitative and colored graphical representation of both ELF and LOL analyses respectively. In these figures, the color red denotes high ELF and LOL values, while the color blue denotes the location with the lowest ELF and LOL value and also these colors (red and blue) are represented localization and delocalization of electrons respectively. As shown from Figure 5(a) and (b), in the present investigation the red region around H43, H34, H33, H40, H45 are projected to be bonding and non-bonding localized electrons because they show the highest LOL and ELF values. The blue color regions at C26, C21, C16, C14, C17, N3, C7, C15, C23, O2 which indicate that delocalization of electrons around the nucleus and also specific blue circles are found at C21, C14 and C7, give high electron delocalization around the nucleus. Since these highest delocalization regions N5–C21 = O2, C14–S1–C11 and C7 = C8–N3 were also presented graphically in Figure 6.

The RDG graph is being used to detect weak inter and intra molecular interactions among the atoms of the molecule and this graph was plotted RDG versus sign $(\lambda_2)\rho$ gives a visualization of
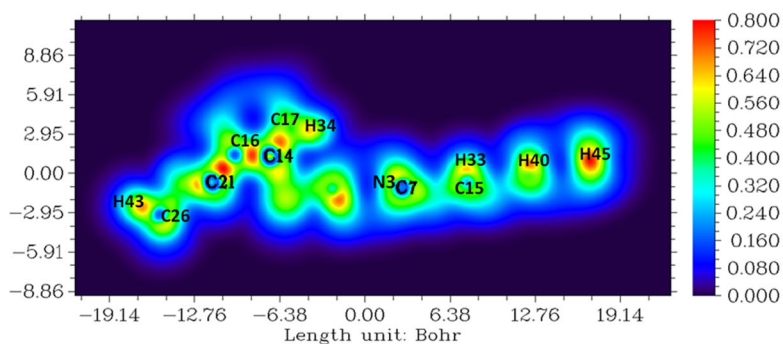
**(a)**
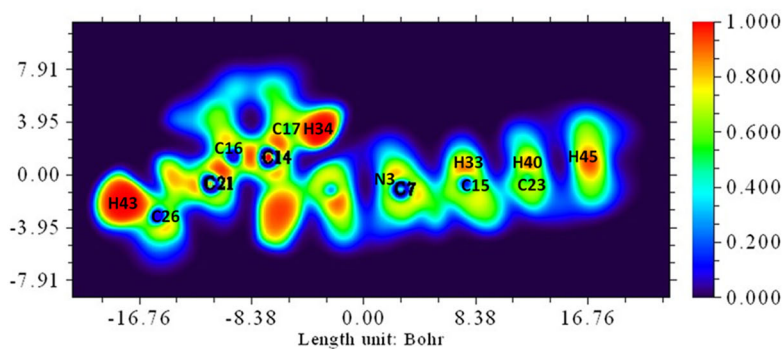
(b)

Figure 5. 2D Plot of Electron localization function (ELF) for important delocalization regions (a) C14–S1–C11, (b) N5–C21 = O2.
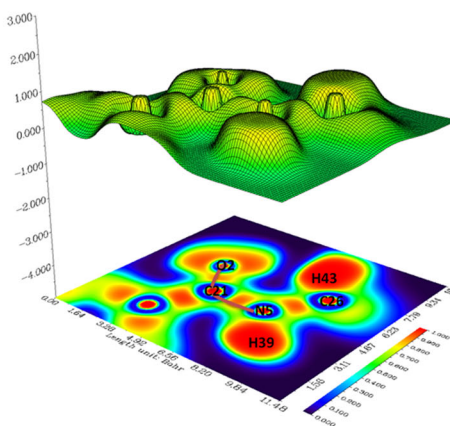
weak interactions in a small range. Weak interactions in the molecule with its surroundings are observed using non-covalent interactions (NCI) and a continuation of AIM analysis. The energy equation can be used to determine the RDG values for the scatter plot,[76] RDG® = $1/2(3\pi^2)^{1/3}|\nabla \rho(r)|/\rho(r)^{4/3}$, where $\rho(r)$ is the electron density. According to this hypothesis, the materials' attractive, repulsive and neutral interactions are represented by the tiny range between negative and positive values of sign $(\lambda_2)\rho$. In the RDG map, if the sign $(\lambda_2)\rho$ value greater than zero $((\lambda_2)\rho > 0)$, nearly zero $((\lambda_2)\rho \approx 0)$ and less than zero $((\lambda_2)\rho < 0)$ are indicating that the repulsive steric effect, Van der Waals (vdW) interactions and the attractive hydrogen bond interaction, respectively, and their corresponding colors of red, green and blue were also used to identify them. In the present study, from Figure 7, the sign $(\lambda_2)\rho$ region (−0.01 to −0.018 a.u) of dark green with slightly blue color spikes implies that Van der Walls interactions at C14–S1 … O2 and the intra molecular hydrogen bond at C13–C11 … H34, respectively. The region above 0.01a.u (0.01 to 0.02 a.u & ≈ 0.05 a.u) of red color spikes represents strong steric repulsive effect.

Molecular docking and simulations

Due to the antitumor activity of MPSB, docking is done with the PDBs, 3AGC, 7BT5, 1NCO, 5UAB, 6FFJ and 6OSH with AutoDock software.[77,78] The PDBs have crystal structures having resolutions 1.12–2.49 Å and are antitumor protein complexes.[79–83] 6FFJ is a 2.20 Å crystal structure of anti-tumor 14F7 derived single-chain Fvs.[83] 6OSH is a 1.12 Å crystal structure of an
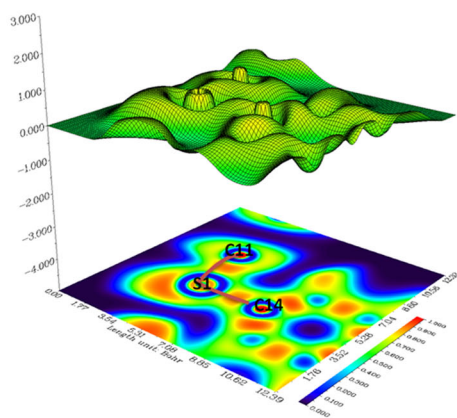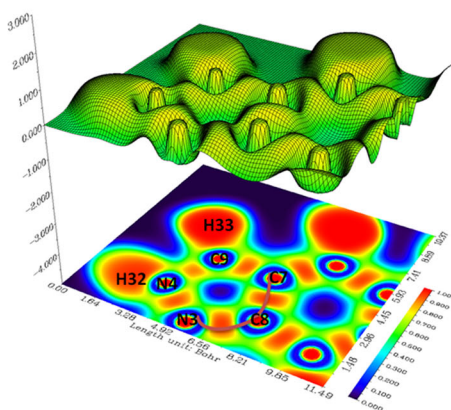
Figure 6. AIM Molecular graph of MPSB: green small spheres (BCPs), small red sphere (RCBs), black lines (bond paths), ash color solid lines (RCP to BCP ring path) and block dotted lines (non-covalent weak interactions).
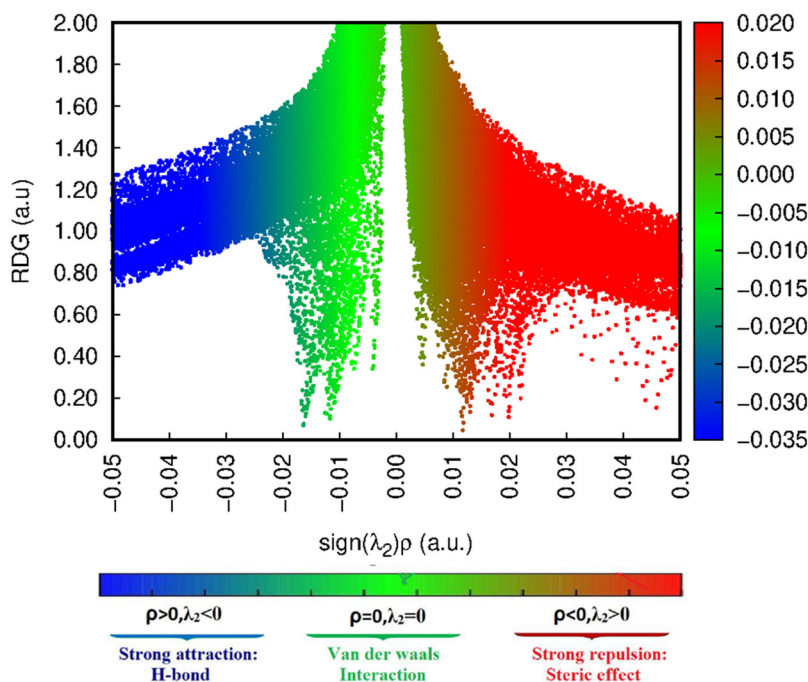
Figure 7. RDG Plots versus the electron density ρ multiplied by the sign of $\lambda 2$ for MPSB.

antitumor antibody complex with tyrosine-protein kinase trans-membrane receptor ROR2.[84] The binding energies are respectively, -10.9, -9.9, -8.8, -8.5, -8.2 and -8.1 kcal/mol for the MPSB complex with 3AGC, 7BT5, 1NCO, 5UAB, 6FFJ and 6OSH and results in suitable inhibitory activity against the receptors and hence the title compound can be developed as a multidrug. The 2D interaction plots (Figure S6) with the amino acids of the PDBs are generated by using BIOVIA Discovery Studio software (http://accelrys.com/products/collaborative-science/biovia-dis-covery-studio/).

Interactions of 3AGC with MPSB: The active amino acid Arg215 forms conventional H-bond and carbon-hydrogen bond with same carbonyl group having 2.73, 2.54 Å. Arg215 also forms hydrophobic amide π-stacked interaction with 1,2-disubstiuted phenyl ring and hydrophobic π-alkyl interaction with five member ring showing the distances 3.87, 3.70, respectively. Arg279 shows an electrostatic π-cation interaction and His 171 shows a hydrophobic π–π T-shaped interaction with pyridine are at the distances of 4.59, 4.56 Å. Pro220 displays two hydrophobic π-alkyl interactions with the phenyl rings at distances of 4.87, 5.42 Å. Val 208 formulate hydrophobic π-alkyl interaction with 1,2-disubstiued phenyl ring at the distance of 5.15 Å.

In our study, the crystal structure of F218V mutant of the substrate-bound red chlorophyll catabolite reductase apo and complex with selected ligands from docking LIG was subjected to molecular dynamics simulation analysis due to the high docking energy of -10.9 kcal/mol. MD simulation for 100 ns was conducted to understand the stability of the above-mentioned protein-ligand complexes root mean square deviation (RMSD), root mean square fluctuations (RMSF), RG, H-bonds (Hydrogen bonds) and MMPSA calculations were made.

Root mean square deviation is an important parameter for the determination of the differences between the two confirmations. The higher the RMSD value, the more is the deviation. The RMSD values are calculated against the simulation timescale of 20–100 ns. The average RMSDs from 0 to 100 ns for apo and ligand–protein were 0.35 and 0.37 nm which gives relative stability
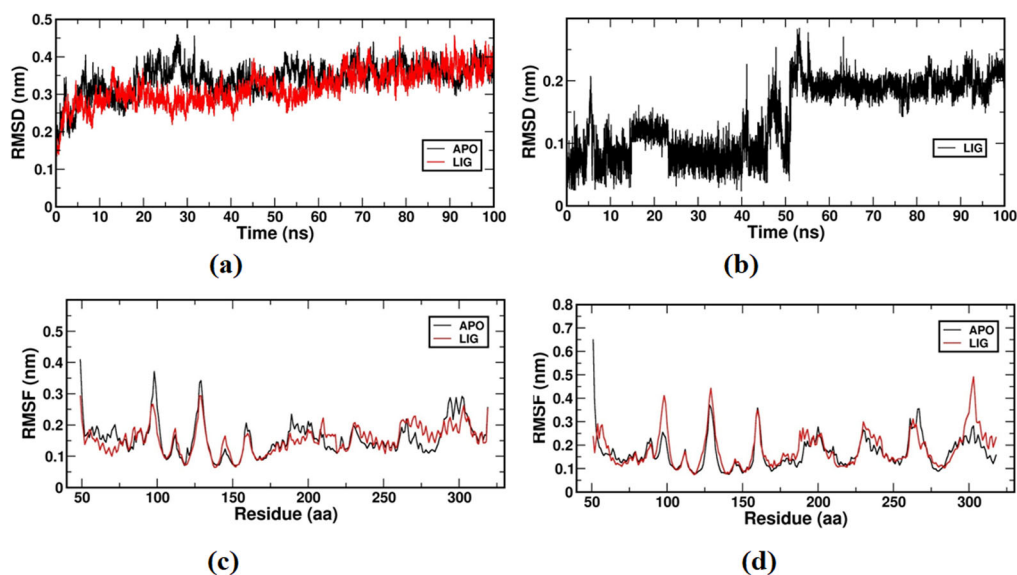
Figure 8. (a) RMSD of backbone atoms of apo and its complex with ligand complex, (b) ligand RMSD of backbond atoms of ligand complex, (c) RMSF of c-alpha atoms of apo and its complex with ligand with chain A, (d) RMSF of c-alpha atoms of apo and its complex with ligand with chain B.

of apo and ligand complex.[85] RMSD results for APO and its complex with the ligand are depicted in Figure 8. During the 100 ns simulation, it was observed that the APO and complexes are equilibrated after 20 ns of time. The mean RMSD of apo and complexes were calculated from 20 ns to 100 ns. The amino acids involved in bringing the overall structural deviation are explored in the RMSF plots.

Ligand RMSD is an important parameter for the determination of the differences between the two confirmations. The Ligand RMSD values are calculated against the simulation timescale of 0 to 100 ns. The average ligand RMSDs from 0 to 100 ns for inhibitors ligand was 0.17 nm, giving a good stability.[86]

RMSF analysis determines which amino acids of the protein make more vibrations, resulting in the destabilization of protein in the presence and absence of the ligands. The RMSF values are calculated against the simulation timescale of 0–100 ns. The RMSF results for APO and its complex with ligand, chain A and chain B are depicted in Figure 8. The average RMSF-A chain and B chain from 0 to 100 ns for apo and ligand complex were 0.3 nm, respectively.

The compactness of the protein can be determined by the radius of gyration. Folding and unfolding of the protein was analyzed by the RG values against the simulation timescale of 0 to 10,000 ps for APO and its complex with ligand. The average RG from 0 to 100 ns for apo and ligand complexes were 2.59 and 2.62 nm. The RG result of the APO and its complex with ligand is depicted in Figure 9.

To understand the modulation of inhibitors on the protein, SASA changes the compactness of protein. In all of the complexes, the changes in SASA values were relatively small. SASA values range from 0 to 100 represented in Figure 9 with an average from 0 to 100 ns for apo and inhibitors ligand were 262 and 269, respectively.[87] Protein–ligand complexes are stabilized by the formation of hydrogen bonds. In our research, the hydrogen bonds formed in the molecular docking analysis are confirmed by the simulation analysis. The H-bond result of the complex with ligand (Figure 9). How much energy is required for the ligands to bind to protein is determined by MMPBSA. The binding energy of ligand is -115.757 ± 14.212 kJ/mol and MMPSA of the complex with the ligand of last 20 ns simulation
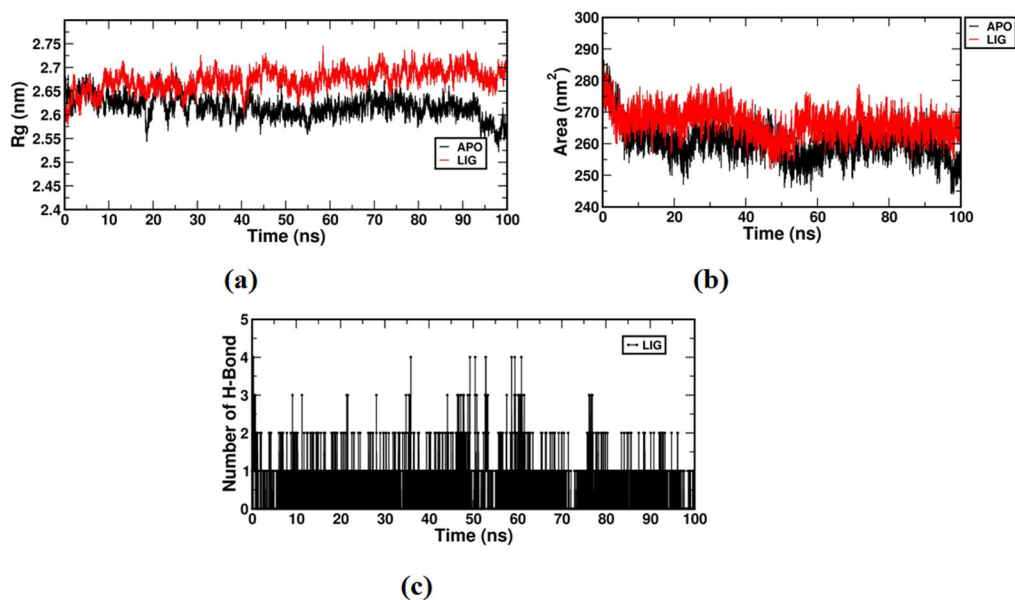
Figure 9. (a) RG of backbone atoms of apo and its complex with ligand, (b) SASA of backbone atoms of apo and its complex with ligand, (c) H-bond of complex with ligand.

Conclusion

The quantum mechanical properties of the drug molecule, MPSB with the intention to illustrate its various physicochemical properties, are reported in the present work. The FMOs together with MEP analysis helped to study the relative stability and activity of the compound. The positive value of Laplacian electron density are 0.0560 and 0.0469 a.u. at S1–O2 and C11–H34 which shows that the closed-shell weak interactions of electrostatic nature and other negative values of density represents a strong covalent bond interaction.

The highest bond ellipticity value was noted at C11–H34, which exhibits the greater asymmetry of electron density distribution and π-bond nature of the title compound. The mean RMSD, RMSF and RG values of apo and complexes were calculated from 20 to 100 ns and the amino acids involved in bringing the overall structural deviation are explored in the RMSF plots. The binding energy of the ligand was -115.757 ± 14.212 kJ/mol.

Disclosure statement

No potential conflict of interest was reported by the authors.

Acknowledgments

References

1. A. Dore, B. Asproni, A. Scampuddu, G. A. Pinna, C. T. Christoffersen, M. Langgard, and J. Kehler, "Synthesis and SAR Study of Novel Tricyclic Pyrazoles as Potent Phosphodiesterase 10A Inhibitors," *European Journal of Medicinal Chemistry* 84 (2014): 181–93. 10.1016/j.ejmech.2014.07.020.

2. D. F. Bonafoux, S. L. Bonar, M. Clare, A. M. Donnelly, J. L. Glaenzer, J. A. Guzova, H. Huang, N. N. Kishore, F. J. Koszyk, P. J. Lennon, et al, "Aminopyridinecarboxamide-Based Inhibitors: Structure-Activity Relationship," *Bioorganic & Medicinal Chemistry* 18, no. 1 (2010): 403–14. 10.1016/j.bmc.2009.10.040.

3. P. Gautam, D. Gautam, and R. P. Chaudhary, "Experimental and Theoretical Investigations on Acid Catalysed Tereoselective Synthesis of New Indazolyl-Thiazole Derivatives," *Journal of Molecular Structure* 1160 (2018): 333–41. 10.1016/j.molstruc.2018.02.003.

4. M. Pordel, S. A. Beyramabadi, and A. Mohammadinejad, "Synthesis, DFT Calculations and Cyclic Voltammetry Analysis of New Heterocyclic Green Dyes: 2-(5-Hydroxyimino-1-Alkyl-4,5-Dihydro-1H-4-Indazolyliden)-2-Arylacetonitriles," *Dyes and Pigments* 102 (2014): 46–52. 10.1016/j.dyepig.2013.10.021.

5. E. Alikhani, M. Pordel, and L. R. Daghigh, "Pyrazolo[4,3-a]Quinindoline as a New Highly Fluorescent Heterocyclic System: Design, Synthesis, Spectroscopic Characterization and DFT Calculations," *Spectrochimica Acta* 136 (2015): 1484–90. 10.1016/j.saa.2014.10.040.

6. S. Poorhaji, M. Pordel, and S. Ramezani, "New Heterocyclic Green, Blue and Orange Dyes from Indazole: Synthesis, Tautomerism, Alkylation Studies, Spectroscopic Characterization and DFT/TD-DFT Calculations," *Journal of Molecular Structure* 1119 (2016): 151–6. 10.1016/j.molstruc.2016.04.078.

7. J. K. Park, W. K. Shin, and D. K. An, "New and Efficient Synthesis of Amides from Acid Chlorides Using Diisobutyl (Amino) Aluminium," *Bulletin of the Korean Chemical Society* 34, no. 5 (2013): 1592–4. 10.5012/bkcs.2013.34.5.1592.

8. R. M. Lanigan, P. Starkov, and T. D. Sheppard, "Direct Synthesis of Amides from Carboxylic Acids and Amines Using B(OCH$_2$CF$_3$)$_3$," *The Journal of Organic Chemistry* 78, no. 9 (2013): 4512–23. 10.1021/jo400509n.

9. R. Tang, L. Jin, C. Mou, J. Yin, S. Bai, D. Hu, J. Wu, S. Yang, and B. Song, "Synthesis, Antifungal and Antibacterial Activity for Novel Amide Derivatives Containing a Triazole Moiety," *Chemistry Central Journal* 7, no. 1 (2013): 30–6. 10.1186/1752-153X-7-30.

10. D. Rai and R. K. Sing, "Synthesis and Antibacterial Activity of Benzamides and Sulfonamide Derived from 2-Amino-5-Bromo/Nitropyridine against Bacterial Strains Isolated from Clinical Patients," *Indian Journal of Chemistry* 50B, no. 7 (2011): 931–6. https://nopr.niscair.res.in/handle/123456789/12098.

11. Y. F. Xiang, C. W. Qian, G. W. Xing, J. Hao, M. Xia, and Y. F. Wang, "Anti-Herpes Simplex Virus Efficacies of 2-Aminobenzamide Derivatives as Novel HSP90 Inhibitors," *Bioorganic & Medicinal Chemistry Letters* 22, no. 14 (2012): 4703–6. 10.1016/j.bmcl.2012.05.079.

12. J. F. Lu, P. Huang, D. Zhang, Q. Wang, N. Zheng, R. Wu, Q. Liu, L. X. Jin, X. H. Yu, X. H. Ji, et al, "1-(3-Amino-4-Morpholino-1H-Indazole-1-Carbonyl)-N-Phenylcyclopropane-1-Carboxamide: Design, Synthesis, Crystal Structure, Antitumor Activity, DFT and Hirshfeld Surface Analysis," *Journal of Molecular Structure* 1210 (2020): 127996. 10.1016/j.molstruc.2020.127996.

13. K. Park, B. M. Lee, K. H. Hyun, T. Han, D. H. Lee, and H. H. Choi, "Design and Synthesis of Acetylenyl Benzamide Derivatives as Novel Glucokinase Activators for the Treatment of t2dm," *ACS Medicinal Chemistry Letters* 6, no. 3 (2015): 296–301. 10.1021/ml5004712.

14. N. Charaya, D. Pandita, A. S. Grewal, and V. Lather, "Design, Synthesis and Biological Evaluation of Novel Thiazol—2yl Benzamide Derivatives as Glucokinase Activators," *Computational Biology and Chemistry* 73 (2018): 221–9. 10.1016/j.compbiolchem.2018.02.018.

15. A. S. Grewal, R. Kharb, D. N. Prasad, J. S. Dua, and V. Lather, "Design, Synthesis and Evaluation of Novel 3,5-Disubstiuted Benzamide Derivatives as Allosteric Glucokinase Activators," *BMC Chemistry* 13 (2019): 1–14. 10.1186/s13065-019-0532-8.

16. Z. Wang, X. Shi, H. Zhang, L. Yu, Y. Cheng, H. Zhang, H. Zhang, J. Zhou, J. Chen, X. Shen, et al, "Discovery of Cycloalkyl-Fused N-thiazol-2-yl-benzamides as Tissue Non-specific Glucokinase Activators: Design, Synthesis, and Biological Evaluation ," *European Journal of Medicinal Chemistry* 139 (2017): 128–52. 10.1016/j.ejmech.2017.07.051.

17. A. S. Grewal, S. Singh, D. Pandita, and V. Lather, "Design, Synthesis and Antidiabetic Activity of Novel Sulfamoyl Benzamide," *Journal of Pharmaceutical Technology, Research and Management* 6 (2018): 115–24. 10.15415/jptrm.2018.62008.

18. E. O. Ibnouf, A. Kaiba, M. H. Geesi, A. M. Alghamdi, Z. S. Aldajani, O. Dehbi, P. Guionneau, R. Azzallou, and Y. Riadi, "Synthesis, Antibacterial Evaluation, Crystal Structure, Molecular Interaction Analysis and DFT Calculations of Novel N-Hydroxy-2-(4-Methylbenzmido)Benzamide," *Journal of Molecular Structure* 1246 (2021): 131214. 10.1016/j.molstruc.2021.131214.

19. M. J. Ahsan, R. K. Kumawat, S. S. Jadav, M. H. Geesi, M. A. Bakht, M. Z. Hassan, A. B. Saleh Al-Tamimi, Y. Riadi, S. A. Hussain, N. M. Ganta, et al, "Synthesis, Cytotoxic Evaluation and Molecular Docking Studies of N-(7-Hydroxy-4-Methyl-2-Oxoquinolin-1(2H)Acetamide/Benzamide Analogues," *Letters in Drug Design and Discovery* 16 (2019): 182–93. 10.2174/1570180815666180501160047.

20. A. Dwivedi, and A. Kumar, "Molecular Docking and Comparative Vibrational Spectroscopic Analysis, HOMO-LUMO, Polarizabilities, and Hyperpolarizabilities of N-(4-Bromophenyl)-4-Nitrobenzamide by

Different DFT (B3LYP, B3PW1 and MPW1PW91) Methods," *Polycyclic Aromatic Compounds* 41, no. 2 (2021): 387–99. https://doi.org/10.1080/10406638.2019.1591466

21. M. A. Patharia, S. V. Raut, B. K. Dhotre, and M. A. Pathan, "Design, Synthesis of Some New N-(2-Fluoro-4-Morpholin-4-yl-Phenyl)-Substituted-Benzamide Derivatives and Screening of Their Microbial Activities," *Polycyclic Aromatic Compounds* (2020). 10.1080/10406638.2020.1833047.

22. H. Fujieda, M. Kogami, M. Sakairi, N. Kato, M. Makino, N. Takahashi, T. Miyazawa, S. Harada, and T. Yamashita, "Discovery of a Potent Glucokinase Activator with a Favorable Liver and Pancreas Distribution Pattern for the Treatment of Type 2 Diabetes Mellitus," *European Journal of Medicinal Chemistry* 156 (2018): 269–94. 10.1016/j.ejmech.2018.06.060.

23. A. M. Deshpande, D. Bhuniya, S. De, B. Dave, V. P. Vyavahare, S. H. Kurhade, S. R. Kandalkar, K. P. Nai, B. S. Kobal, R. D. Kaduskar, et al, "Discovery of Liver-Directed Glucokinase Activator having Anti-Hyperglycemic Effect without Hypoglycemia ," *European Journal of Medicinal Chemistry* 133 (2017): 268–86..

24. S. C. Khadse, N. D. Amnerkar, K. S. Dighole, A. M. Dhote, V. R. Patil, D. K. Lokwani, V. G. Ugale, N. B. Charbe, and V. A. Chatpalliwar, "Hetero-Substituted Sulfonamide-Benzamide Hybrids as Glucokinase Activators: Design, Synthesis, Molecular Docking and in Silico ADME Evaluation," *Journal of Molecular Structure* 1222 (2020): 128916. 10.1016/j.molstruc.2020.128916.

25. S. Malasala, M. N. Ahmad, J. Gour, M. Shukla, G. Kaul, A. Akhir, S. Gatadi, Y. V. Madhavi, S. Chopra, and S. Nanduri, "Synthesis, Biological Evaluation and Molecular Modeling Insights of 2-Arylquinazoline Benzamide Derivatives as anti-Tubercular Agents," *Journal of Molecular Structure* 1218 (2020): 128493. https://doi.org/10.1016/j.molstruc.2020.128493.

26. R. Sharma, J. Joubert, H. Su, M. R. Caira, and S. F. Malan, "Synthesis, Crystal Structure, DFT Studies and Biological Evaluation of N-Benzamido Derivatives of Oxahexacycloundecyl Amines: A Case of Enantiomerism Leading to Molecular Disorder," *Journal of Molecular Structure* 1215 (2020): 128248. 10. 1016/j.molstruc.2020.128248.

27. M. M. Goldenber, "Celecoxib, a Selective Cyclooxygenase-2 Inhibitor for the Treatment of Rheumatoid Arthritis and Osteoarthritis," *Clinical Therapeutics* 21 (1999): 1497–513..

28. A. I. Graul, E. Cruces, E. Dulsat, E. Arias, and M. Stringer, "The Year's New Drugs and Biologics," *Drugs of Today* 48, no. 1 (2012): 33. 10.1358/dot.2012.48.1.1769676.

29. R. M. Young, and L. M. Staudt, "Ibrutinib Treatment of CLL: The Cancer Fights Back," *Cancer Cell* 26, no. 1 (2014): 11–3. 10.1016/j.ccr.2014.06.023.

30. J. J. Cui, M. Tran-Dube, H. Shen, M. Nambu, P. P. Kung, M. Pairish, L. Jia, J. Meng, L. Funk, I. Botrous, M. McTigue et al., "Structure Based Drug Design of Crizotinib (PF-02341066), a Potent and Selective Dual Inhibitor of Mesenchymal-Epithelial Transition Factor (c-MET) Kinase and Anaplastic Lymphoma Kinase (ALK) enzylsulf)," *Journal of Medicinal Chemistry* 54, no. 18 (2011): 6342–63. 10.1021/jm2007613

31. L. P. H. Yang and K. McKeage, "Axitinib: In Advanced, Treatment-Experienced Renal Cell Carcinoma," *Drugs* 72, no. 18 (2012): 2375–84.10.2165/11209230-000000000-00000.

32. E. Polo, L. Prent-Peñaloza, Y. A. R. Núñez, L. Valdés-Salas, J. Trilleras, J. Ramos, J. A. Henao, A. Galdámez, A. Morales-Bayuelo, and M. Gutiérrez, "Microwave-Assisted Synthesis, Biological Assessment, and Molecular Modeling of Aza-Heterocycles: Potential Inhibitory Capacity of Cholinergic Enzymes to Alzheimer's Disease," *Journal of Molecular Structure* 1224 (2021): 129307. 10.1016/j.molstruc.2020.129307.

33. M. Fukudo, G. Tamaki, M. Azumi, H. Kakizaki, S. Matsumoto, and Y. Tasaki, "Absorption of the Orally Active Multikinase Inhibitor Axitinib as a Therapeutic Index to Guide Dose Titration in Metastatic Renal Cell Carcinoma," *Investigational New Drugs* 39, no. 2 (2021): 595–604. 10.1007/s10637-020-01023-z.

34. B. I. Rini, E. R. Plimack, V. Stus, R. Gafanov, R. Hawkins, D. Nosov, F. Pouliot, B. Alekseev, D. Soulieres, B. Melichar, I. Vynnychenko, et al, "Pembrolizumab plus Axitinib versus Sunitinib for Advanced Renal-Cell Carcinoma," *New England Journal of Medicine* 380, no. 12 (2019): 1116–27. 10.1056/NEJMoa1816714.

35. M. Vasileiadis, C. C. Pantelides, and C. S. Adjiman, "Prediction of the Crystal Structures of Axitinib, a Polymorphic Pharmaceutical Molecule," *Chemical Engineering Science* 121 (2015): 60–76. 10.1016/j.ces.2014. 08.058.

36. R. Pedrosa, C. Andres, J. P. Duque-Soladana, A. Maestro, and J. Nieto, "Regio- and Diastereoselective Tandem Addition-Carbocyclization Promoted by Sulfanyl Radicals on Chiral Perhydro-1,3-Benzoxazines," *Tetrahedron: Asymmetry.* 14, no. 19 (2003): 2985–90. 10.1016/j.tetasy.2003.06.003.

37. S. Narayanan, N. A. Gujarati, J.-Q. Wang, Z.-X. Wu, J. Koya, Q. Cui, V. L. Korlipara, C. R. Ashby Jr, and Z. S. Chen, "The Novel Benzamide Derivative, VKNG-2, Restores the Efficacy of Chemotherapeutic Drugs in Colon Cancer Cell Lines by Inhibiting the ABCG2 Transporter," *International Journal of Molecular Sciences* 22, no. 5 (2021): 2463. 10.3390/ijms22052463.

38. P. Peluso and B. Chankvetadze, "The Molecular Bases of Chiral Recognition in 2-(Benzylsulfinyl)Benzamide Enantioseparation," *Analytica Chimica Acta* 1141 (2021): 194–205. 10.1016/j.aca.2020.10.050.

39.   J. Zhang, H. Xiong, F. Yang, J. He, T. Chen, D. Fu, P. Zheng, and Q. Tang, "Design, Synthesis and Biological Evaluation of Novel 4-(pyrrolo[2,3-d]pyrimidine-4-yloxy)benzamide Derivatives as Potential Antitumor Agents ," *Bioorganic & Medicinal Chemistry Letters* 33 (2021): 127740 https://doi.org/10.1016/j.bmcl.2020.127740

40.   G. Routholla, S. Pulya, T. Patel, S. A. Amin, N. Adhikari, S. Biswas, T. Jha, and B. Ghosh, "Synthesis, Biological Evaluation, and Molecular Docking Analysis of Novel Linker-less Benzamide based Potent and Selective HDAC3 inhibitors ," *Bioorganic chemistry* 114 (2021): 105050. 10.1016/j.bioorg.2021.105050.

41.   C. Y. Panicker, A. Raj, H. T. Varghese, K. Raju, and Y. S. Mary, "Vibrational sSpectroscopic sStudies and cComputational sStudy of mMethyl-(2-mMethyl-4,6-dDinitrophenyl sSulfanyl)eEthanoate," *Journal of Raman Spectroscopy* 41, no. 7 (2010): 829–38. 10.1002/jrs.2509.

42.   A. Raj, Y. S. Mary, C. Y. Panicker, H. T. Varghese, and K. Raju, "IR, Raman, SERS and Computational Study of 2-(Benzylsulfanyl)-3,5-Dinitrobenzoic acienzylsulfinyl ," *Spectrochimica Acta Part A, Molecular and Biomolecular Spectroscopy* 113 (2013): 28–36. 10.1016/j.saa.2013.04.096.

43.   N. Z. Alzoman, Y. S. Mary, C. Y. Panicker, I. A. Al-Swaidan, A. A. El-Emam, O. A. Al-Deeb, A. A. Al-Saadi, C. Van Alsenoy, and J. A. War, "Spectroscopic Investigation (FT-IR and FT-Raman), Vibrational Assignments, HOMO-LUMO, NBO, MEP Analysis and Molecular Docking Study of 2-[(4-Chlorobenzyl)Sulfanyl]-4-(2-Methylpropyl)-6-(Phenylsulfanyl)-Pyrimidine-5-Carbonitrile, a Potential Chemotherapeutic Agent," *Spectrochimica Acta Part A, Molecular and Biomolecular Spectroscopy* 139 (2015): 413–24. doi: 10.1016/j.saa.2014.12.043.

44.   P. Horcajada, T. Chalati, C. Serre, B. Gillet, C. Sebrie, T. Baati, J. F. Eubank, D. Heurtaux, P. Clayette, C. Kreuz et al., "Porous Metal-Organic-Framework Nanoscale Carriers as a Potential Platform for Drug Delivery and Imaging," *Nature Materials* 9, no. 2 (2010): 172–8. 10.1038/nmat2608.

45.   H. Hakkinen, "The Gold-Sulfur Interface at the Nanoscale," *Nature Chemistry.* 4 (2012): 443–55. 10.1038/nchem.1352.

46.   K. B. Bhavitha, A. K. Nair, S. Perumbilavil, S. Joseph, M. S. Kala, A. Saha, R. A. Narayanan, N. Hameed, S. Thomas, O. S. Oluwafemi et al., "Investigating Solvent Effects on Aggregation Behavior, Linear and Nonlinear Optical Properties of Silver Nanoclusters," *Optical Materials* 73 (2017): 695–705. 10.1016/j.optmat.2017.09.024.

47.   B. Yin and Z. Luo, "Coinage Metal Clusters: From Superatom Chemistry to Genetic Materials," *Coordination Chemistry Reviews* 429 (2021): 213643. 10.1016/j.ccr.2020.213643.

48.   J. S. Al-Otaibi, Y. S. Mary, Y. S. Mary, Z. Ullah, and H. W. Kwon, "Adsorption Behavior and Solvent Effects of an Adamantane-Triazole Derivative on Metal Clusters-DFT Simulation Studies," *Journal of Molecular Liquids.* 345 (2022): 118242. 10.1016/j.molliq.2021.118242.

49.   M. J. Frisch, G. W. Trucks, H. B. Schlegel, G. E. Scuseria, M. A. Robb, J. R. Cheeseman, G. Scalmani, V. Barone, G. A. Petersson, H. Nakatsuji, et al., *Gaussian 16, Revision A.03* (Wallingford CT: Gaussian, Inc., 2016).

50.   K. Raghavachari, J. S. Binkley, R. Seeger, and J. A. Pople, "Self-Consistent Molecular Orbital Methods. 20. Basis Set for Correlated Wave-Function," *Journal of Chemical Physics* 72 (1980): 650–4. 10.1063/1.438955.

51.   R. Dennington, T. A. Keith, and J. M. Millam, *GaussView, Version 6.1* (Shawnee Mission, KS: Semichem Inc., 2016).

52.   T. Lu and F. Chen, "Multiwfn: A Multifunctional Wavefunction Analyzer," *Journal of Computational Chemistry* 33, no. 5 (2012): 580–92. 10.1002/jcc.22885.

53.   J. A. Lemkul, W. J. Allen, and D. R. Bevan, "Practical Consideration for Building GROMOS-Compatible Small Molecule Topologies," *Journal of Chemical Information and Modeling* 50, no. 12 (2010): 2221–35. 10.1021/ci00335w.

54.   B. S. Gangadharappa, R. Sharath, P. D. Revanasiddappa, V. Chandramohan, M. Balasubramaniam, and T. P. Vardhineni, "Structural Insights of Metallo-Beta-Lactamase Revealed an Effective Way of Inhibition of Enzyme by Natural Inhibitors," *Journal of Biomolecular Structure & Dynamics* 38, no. 13 (2020): 3757–71. 10.1080/07391102.2019.1667265.

55.   Rashmi Kumari, Rajendra Kumar, and Andrew Lynn, "Open Source Drug Discovery Consortium g_mmpbsa-a GROMACS tool for high-throughput MM-PBSA calculations ," *Journal of Chemical Information and Modeling* 54, no. 7 (2014): 1951–62. 10.1021/ci500020m.

56.   G. Kresse and J. Hafner, "Ab Initio Molecular Dynamics for Liquid Metals," *Physical Review B Condensed Matter* 47, no. 1 (1993): 558–61. 10.1103/physrevb.47.558.

57.   G. Kresse and J. Furthmuller, "Efficient Iterative Schemes for ab Initio Total-Energy Calculations using a Plane-Wave Basis Set ," *Physical Review. B, Condensed Matter* 54, no. 16 (1996): 11169–86. 10.1103/physrevb.54.11169.

58.   G. Kresse and D. Joubert, "From Ultrasoft Pseudopotentials to the Projector," *Physical Review B* 59, no. 3 (1999): 1758–75. 10.1103/physrevc.59.1758.

59. P. E. Blochl, "Projector Augmented-Wave Method," *Physical Review* 50 (1994): 17953. 10.1103/physrevb.50.17953.

60. K. Haruna, V. S. Kumar, Y. S. Mary, S. A. Popoola, R. Thomas, M. S. Roxy, and A. A. Al-Saadi, "Conformational Profile, Vibrational Assignments, NLO Properties and Molecular Docking of Biologically Active herbicide1,1-dimethyl-3-phenylurea ," *Heliyon* 5, no. 6 (2019): https://doi.org/10.1016/j.heliyon.2019.e01987

61. J. S. Al-Otaibi, A. H. Almuqrin, Y. S. Mary, and R. Thomas, "Modeling the Conformational Presence, Spectroscopic Properties, UV Light Harvesting Efficiency, Biological Receptor Inhibitory Ability and Other Physic-Chemical Properties of Five Imidazole Derivatives Using Quantum Mechanical and Molecular Mechanics Tools," *Journal of Molecular Liquids* 310 (2020): https://doi.org/10.1016/j.molliq.2020.112871

62. R. I. Al-Wabli, K. S. Resmi, Y. S. Mary, C. Y. Panicker, M. I. Attia, A. A. El-Emam, and C. Van Alsenoy, "Vibrational Spectroscopic Studies, Fukui Functions, HOMO-LUMO, NLO, NBO Analysis and Molecular Docking Stud© (E)-1-(1,3-Benzodioxol-5-yl)-4,4-Dimethylpent-1-en-3-One, a Potential Precursor to Bioactive Agents," *Journal of Molecular Structure.* 1123 (2016): 375–83. https://doi.org/10.1016/j.molstruc.2016.07.044

63. Y. S. Mary, Y. S. Mary, K. S. Resmi, and R. Thomas, "DFT and Molecular Docking Investigations of Oxicam derivatives," *Heliyon* 5, no. 7 (2019): https://doi.org/10.1016/j.heliyon.2019.e02175

64. V. V. Aswathy, S. Alper-Hayta, G. Yalcin, Y. S. Mary, C. Y. Panicker, P. J. Jojo, F. Kaynak-Onurdag, S. Armakovic, S. J. Armakovic, I. Yildiz, et al, "Modification of Benzoxazole Derivative by Bromine-Spectroscopic, Antibacterial and Reactivity Study Using Experimental and Theoretical Procedures," *Journal of Molecular Structure* 1141 (2017): 495–511. 10.1016/j.molstruc.2017.04.010.

65. E. D. Glendening, A. E. Reed, J. E. Carpenter, and F. Weinhold N. B. O. Version, 3.1, TCI (Madison: University of Wisconsin, , 1998).

66. S. Beegum, Y. S. Mary, H. T. Varghese, C. Y. Panicker, S. Armakovic, S. J. Armakovic, J. Zitko, M. Dolezal, and C. Van Alsenoy, "Vibrational Spectroscopic Analysis of Cyanopyrazine-2-Carboxamide Derivatives and Investigation of Their Reactive Properties by DFT Calculations and Molecular Dynamics Simulations," *Journal of Molecular Structure.* 1131 (2017): 1–15. https://doi.org/10.1016/j.molstruc.2016.11.044

67. G. Henkelman, A. Arnaldsson, and H. Jonsson, "A Fast and Robust Algorithm for Bader Decomposition of Charge Density," *Computational Materials Science.* 36 (2006): 254–360. https://doi.org/10.1016/j.commatsci.2005.04.010

68. '. M. O'boyle, A. L. Tenderholt, and K. M. Langner, "Cclib: A Library for Package-Independent Computational Chemistry Alogorithms," *Journal of Computational Chemistry* 29, no. 5 (2008): 839–45. 10.1002/jcc/20823.

69. K. Sangeetha, S. R. Rajina, M. K. Marchewka, and J. Binoy, "The Study of Inter and Intramolecular Hydrogen Bonds of NLO Crystal Melaminium Hydrogen Malonate Using DFT Simulation, AIM Analysis and Hirshfeld Surface Analysis," *Materials Today: Proceedings* 25 (2020): 307–15. 10.1016/j.matpr.2020.01.526.

70. P. Srinivasan, S. N. Asthana, R. B. Pawar, and P. Kumaradhas, "A Theoretical Charge Density Study on Nitrogen-Rich 4,4',5,5'-Tetranitro-2,2'-bi-1H-Imidazole (TNBI) Energetic Molecule," *Structural Chemistry* 22, no. 6 (2011): 1213–20. 10.1007/s11224-011-9815-y.

71. F. Farsinia, M. Dehestani, and M. Molaei, "Investigation of Structural Stability, Electronic Properties of S-Doped CdSe Using ab Initio Calculations," *Structural Chemistry* 31, no. 2 (2020): 701–8. 10.1007/s11224-019-01449-z

72. S. G. Neogi, A. Das, and P. Chaudhury, "Investigation of Plausible Mechanistic Pathways in Hydrogenation of η5-(C5H5)2Ta(H)=CH2: An Analysis Using DFT and AIM Techniques," *Journal of Molecular Modeling* 20 (2014): 2132. 10.1007/s00894-014-2132-9.

73. G. G. Sheeba, D. Usha, M. Amalanathan, M. Sony, and M. Mary, "Identification of Structure Activity Relation of a Synthetic Drug 2,6-Pyridine Dicarbonitrile Using Experimental and Theoretical Investigation," *Wutan Huatan Jisuan Jishu* XVI, no. XI (2020): 89–113. 10.37896/whjj16.11/341.

74. J. Zhou, L. Zhu, J. Chen, W. Wang, R. Zhang, Y. Li, Q. Zhang, and W. Wang, "Degradation Mechanism for Zearalenone ring-cleavage by Zearalenone hydrolase RmZHD: A QM/MM study ," *The Science of the Total Environment* 709 (2020): 135897. 10.1016/j.scitotenv.2019.135897.

75. C. Sivakumar, V. Balachandran, B. Narayana, V. V. Salian, B. Revathi, N. Shanmugapriya, and K. Vanasundari, "Molecular Spectroscopic Investigation, Quantum Chemical, Molecular Docking and Biological Evaluation of 2-(4-Chlorophenyl)-1-[3-(4-Chlorophenyl)-5-[4-(Propan-2-yl)Phenyl-3,5-Dihydro-1H-Pyrazole-yl]Ethanone," *Journal of Molecular Structure* 1224 (2021): 129010. 10.1016/j.molstruc.2020.129010.

76. M. Maria Julie, T. Prabhu, E. Elamuruguporchelvi, Fazilath Basha Asif, S. Muthu, and Ahmad Irfan, "Structural (Monomer and Dimer), Wavefunctional, NCI Analysis in Aqueous Phase, Electronic and Excited State Properties in Different Solvent Atmosphere© 3-{(E)-[(3,4-Dichlorphenyl)Imino]Methyl}Benzene-1,2-Diol," *Journal of Molecular Liquids* 336 (2021): 10.1016/j.molliq.2021.116335.

77. O. Trott and A. J. Olson, "AutoDockVina: Improving the Speed and Accuracy of Docking with a New Scoring Function, Efficient Optimization and Multithreading," *Journal of Computational Chemistry* 31 (2009): 461. 10.1002/jcc.21334.

78. K. B. Benzon, Y. S. Mary, H. T. Varghese, C. Y. Panicker, S. Armakovic, S. J. Armakovic, K. Pradhan, A. K. Nanda, and C. Van Alsenoy, "Spectroscopic, DFT, Molecular Dynamics and Molecular Docking Study of 1-Butyl-2-(4-Hydroxyphenyl)-4,5-Dimethyl-Imidazole 3-Oxide," *Journal of Molecular Structure* 1134 (2017): 330–44. 10.1016/j.molstruc.2016.12.100.

79. M. Sugishima, Y. Okamoto, M. Noguchi, T. Kohchi, H. Tamiaki, and K. Fukuyama, "Crystal Structures of the Substrate-Bound Forms of Red Chlorophyll Catabolite Reductase: Implications for Site-Specific and Stereospecific Reaction ," *Journal of Molecular Biology* 402, no. 5 (2010): 879–91. 10.1016/j.jmb.2010.08.021.

80. J. Zhou, Z. Huang, L. Zheng, Z. Hei, Z. Wang, B. Yu, L. Jiang, J. Wang, and P. Fang, "Inhibition of plasmodium falciparum Lysyl-tRNA Synthetase via an Anaplastic Lymphoma Kinase Inhibitor," *Nucleic Acids Research* 48, no. 20 (2020): 11566–76. https://doi.org/10.1093/nar/gkaa862

81. K. H. Kim, B. M. Kwon, A. G. Myers, and D. C. Rees, "Crystal Structure of Neocarzinostatin, an Antitumor Protein-Chromophore Complex," *Science* 262, no. 5136 (1993): 1042–6. 10.1126/science.8235619.

82. P. J. Farrell, J. Matuszkiewicz, D. Balakrishna, S. Pandya, M. S. Hixon, R. Kamran, S. Chu, J. D. Lawson, K. Okada, A. Hori, et al, "MET Tyrosine Kinase Inhibition Enhances the Antitumor Efficacy of an HGF Antibody," *Molecular Cancer Therapeutics* 16, no. 7 (2017): 1269–78. 10.1158/1535-7163.MCT-16-0771.

83. K. Bjerregaard-Andersen, H. Johannesen, N. Abdel-Rahman, J. E. Heggelund, H. M. Hoas, F. Abraha, P. A. Bousquet, L. S. Hoydahl, D. Burschowsky, G. Rojas et al, "Crystal Structure of an L Chain Optimised 14F7 anti-Ganglioside Fv Suggests a Unique Tumour-Specificity through an Unusual H-Chain CDR3 Architecture," *Scientific Reports* 8, no. 1 (2018): 10836. 10.1038/s41598-018-28918-5.

84. R. S. Goydel, J. Weber, H. Peng, J. Qi, J. Soden, J. Freeth, H. Park, and C. Rader, "Affinity Maturation, Humanization and co-Crystallization of a Rabbit anti-Human ROR2 Monoclonal Antibody for Therapeutic Applications," *Journal of Biological Chemistry* 295, no. 18 (2020): 5995–6006. 10.1074/jbc.RA120.012791.

85. F. Fazil, M. Smitha, Y. S. Mary, Y. S. Mary, V. Chandramohan, N. Kumar, R. Pavithran, and C. Van Alsenoy, "Structural (SC-XRD), Spectroscopic, DFT, MD Investigations and Molecular Docking Studies of a Hydrazone Derivative," *Chemical Data Collections* 30 (2020): 100588. 10.1016/j.cdc.2020.100588.

86. Y. Sheena Mary, Y. Shyma Mary, Vivek Chandramohan, Naveen Kumar, C. Van Alsenoy, and Maria Cristina Gamberini, "DFT and MD Simulations and Molecular Docking of co-Crystals of Octafluoro-1,4-Diiodobutane with Phenazine and Acridine," *Structural Chemistry* 31, no. 6 (2020): 2525–31. 10.1007/s11224-020-01616-7.

87. M. Smitha, Y. S. Mary, Y. S. Mary, G. Serdaroglu, P. Chowdhury, M. Rana, H. Umamahesvari, B. K. Sarojini, B. J. Mohan, and R. Pavithran, "Modeling the DFT Structural and Reactivity Studies of a Pyrimidine-6-Carboxylate Derivative with Reference to Its Wavefunction-Dependent, MD Simulations and Evaluation for Potential Antimicrobial Activity," *Journal of Molecular Structure* 1237 (2021): 130397. 10.1016/j.molstruc.2021.130397.